Post-transcriptional regulation of aortic calcification in KLOTHO deficient mice: impact of miR-145 and miR-378

Ying Tang[1, *], Tapan A. Shah[1, *, †], Edward J. Yurkow[2], and Melissa B. Rogers[1, ‡]

[1]Rutgers - New Jersey Medical School, Microbiology, Biochemistry, & Molecular Genetics, Newark, NJ

[2]Rutgers University Molecular Imaging Center (RUMIC), Rutgers University, Piscataway, NJ

Running title: *MicroRNA profiles in calcified vs. healthy aorta*

*Co-first authors

†Present Address: Advanced Cell Diagnostics, 7707 Gateway Blvd #200, Newark, CA 94560

‡To whom should correspondence and reprint request be addressed to: Melissa B. Rogers, Ph.D., Microbiology, Biochemistry & Molecular Genetics, Rutgers - NJ Medical School (NJMS), Center for Cell Signaling, Room F1216, 205 South Orange Ave., Newark, NJ 07103. Email: rogersmb@njms.rutgers.edu, telephone: 973 972 2984

Keywords: bone morphogenetic protein (BMP), Klotho, SMAD transcription factor, gene regulation, signaling, cardiovascular, calcification, atherosclerosis, renal physiology, microRNA (miRNA)

Abstract

Atherosclerosis and calcific aortic valve disease are common in the aged as well as in those with kidney disease, diabetes, and high cholesterol. Although cardiovascular calcification is a major pathological feature, calcific molecular mechanisms are poorly understood. High bone morphogenetic protein 2 (BMP2) levels and BMP signaling promote calcification. We sought to identify and restore mechanisms that restrain BMP signaling in healthy cardiovascular tissue. MicroRNAs (miRNAs) post-transcriptionally modulate gene expression *via* the 3' untranslated region and have clinical potential as biomarkers and therapeutic agents. Our goal was to elucidate the role of miRNAs that target BMP signaling during pathological calcification in the *Klotho* mouse model of kidney disease. We generated abundance profiles of miRNAs that normally repress BMP2 and other pro-osteogenic proteins in healthy and calcified mouse aorta. We also demonstrated that restoring normal levels of the miR-145 and miR-378 miRNAs can repress the synthesis of BMP2 and other pro-osteogenic proteins and inhibit pathological calcification *in vivo*. These miRNAs are candidates for "miRNA replacement therapies" in the context of chronic kidney disease and other pro-calcific conditions.

Introduction

The American Heart Association projects that 45% of Americans will have some form of heart and/or vascular

disease by 2035 (1). Calcification of blood vessels reduces their diameter and plasticity and ultimately promotes ischemic events (2). Risk factors that promote both vascular and valvular calcification include aging, renal failure, and male sex; as well as hypercholesterolemia, smoking, and diabetes (3,4). An aging population and the epidemic of obesity ensure that cardiovascular disorders will be a major public health threat for decades to come. Understanding the signaling processes that regulate the behavior of vascular cells will reveal novel approaches to preventing and treating these devastating pathologies.

The BMP signaling pathway is essential for osteogenesis and vascular calcification (4-6). BMP ligands bind BMP receptors (BMPR), which phosphorylate and activate SMAD signaling. SMAD signaling increases transcription of *Runx2* and *Msx2*, leading to increased osteogenic differentiation (4,6,7). Abnormally elevated levels of the pro-osteogenic bone morphogenetic protein 2 (BMP2) and increased BMP signaling are implicated in all forms of pathological cardiovascular calcification. For example, BMP2 is synthesized in human atherosclerotic plaques (8) and calcified stenotic valves (9). Moreover, BMP2 can induce master osteogenic factors such as RUNX2 in human aortic valve interstitial cells (10) and MSX2 in aortic smooth muscle cells (11), induce calcification *in vitro* (10,12-15), and cause ossification within adult diseased valves (15-17) and atherosclerotic plaques (8). Forced synthesis of BMP2 in vascular smooth muscle cells accelerated atherosclerotic calcification in *ApoE* null mice fed a high cholesterol diet (18). Genetic deficiency and pharmacological inactivation of BMP signaling reduced calcification not only in cultured cells (15,19,20) but also in *Ldlr* null mice fed a high-fat diet (21), *Mgp* null mice (22) and *Klotho* mutant mice with renal failure (19).

Given the importance of BMP2 and BMP signaling in cardiovascular calcification, identifying post-transcriptional regulators of BMP signaling may provide new insights and targets for the treatment of cardiovascular disease. To increase potential clinical translatability, we also considered evolutionary conservation. The 3'-untranslated region (3'-UTR) binds regulatory proteins and microRNAs (miRNAs) that influence polyadenylation, translation efficiency, and stability of mRNAs (23). All BMP ligands may be post-transcriptionally regulated. However, the extreme evolutionary conservation of the *Bmp2* 3'-UTR relative to other BMP ligand 3'-UTRs supports a potentially greater role for post-transcriptional mechanisms that are conserved between mouse and man (24-26). MicroRNAs are crucial regulators in cardiovascular pathologies (27). The goal of this study was to compare the profiles of miRNAs that modulate the synthesis of BMP2 and downstream BMP signaling proteins in the aorta of healthy mice relative to mice with pathologically calcified aorta. Our mouse model is a *Klotho* hypomorph that causes dysregulated mineral metabolism (28).

Mice homozygous for *Klotho* mutations have a short lifespan, growth retardation, osteoporosis, atherosclerosis, ectopic calcification, and renal disease. The KLOTHO protein, along with 1,25$(OH)_2$ vitamin D3 and FGF23, tightly regulates phosphate homeostasis (29,30). Deficiency of

KLOTHO leads to renal disease and subsequent hyperphosphatemia and ectopic calcification of soft tissues such as aorta, aortic valves and kidneys (19,30). Restoration of normal KLOTHO levels ameliorates calcification (29). The dramatic calcification of the aorta and other tissues in *Klotho* mutant mice within 6-7 weeks of birth make them experimentally attractive for studying the regulation of the *Bmp2* gene during pathological calcification. Furthermore, understanding the mechanism of aortic calcification in the context of kidney failure is important because 17% of the population over the age of 30 may suffer from this major cardiovascular disease risk factor by 2030 (1).

Our objective was to elucidate a comprehensive profile of miRNAs whose abundance is altered in the calcified aorta of *Klotho* homozygous mutant mice with renal disease. We also demonstrate that selected miRNAs can modulate the BMP2 ligand and proteins involved in BMP signaling and calcification *in vivo*. Finally, we tested if restoration of the abundance of miRNAs that inhibit BMP signaling ameliorated aortic calcification. This study begins to fill a key gap in our understanding of post-transcriptional processes that control BMP signaling and calcification in vascular tissues and provides experimental support for miRNA replacement therapies in cardiovascular disease.

Results

BMP signaling and calcification is elevated in aorta from Klotho homozygous mutant mice

BMP signaling is required for valve calcification in *Klotho* null mice (19). We assessed BMP signaling in the calcified aorta of mice homozygous for the original hypomorphic *Klotho* allele (28). BMP signaling and calcium levels in aorta from control mice that were either wild type ($Kl^{+/+}$) or heterozygous ($Kl^{kl/+}$) for the *Klotho* mutation were compared to the aorta from *Klotho* mutant homozygotes ($Kl^{kl/kl}$). BMP signaling, as assessed by phosphorylation of BMP-specific SMADs, was induced nearly 2-fold in aorta from male and female *Klotho* homozygous mice relative to control mice (Fig. 1A, B; $p = 0.03$). Calcium levels in the aorta from *Klotho* mutant homozygotes also were elevated by over 2-fold in males ($p = 1.4 \times 10^{-6}$) and females ($p = 5.0 \times 10^{-4}$) relative to control aorta (Fig. 1C). PET-CT imaging revealed profound mineralization in the aortic sinus and ascending aorta of *Klotho* mutant ($Kl^{kl/kl}$) mice, but not in a control heterozygous ($Kl^{kl/+}$) littermate (Fig. 1D, E). Together, these results confirmed that homozygosity for the hypomorphic *Klotho* mutation amplifies BMP signaling and calcification in the aorta.

We then tested the hypothesis that increased abundances of aortic RNAs encoding the ligand BMP2 or the BMP signaling intermediaries SMADs 1, 5, or 9 accounted for the increased signaling in the *Klotho* homozygotes. The levels of the *Bmp2* and *Smad1* RNAs were similar to those in control mice (Fig. 2A, B). In contrast, *Smad5* and *9* RNA levels were 1.4 fold and 3.0 fold higher, respectively, in the aorta of *Klotho* homozygotes compared to control mice (Fig. 2C, D, $p < 0.05$ and $p < 0.01$). Although we have yet to rule out differential translation of the *Bmp2* and *Smad1* RNAs, we did not observe disease-associated differences in mRNA abundances. However, the increased abundance of the RNAs encoding the SMAD5 and 9 intracellular

BMP signaling intermediaries indicates that increased transcription and/or stability of messages that encode BMP signaling proteins occurs in the aorta of *Klotho* mutant homozygotes.

MicroRNA profiles differ in the aorta from Klotho homozygous mutant mice

BMP signaling and calcium levels are doubled in the aorta of Klotho homozygotes (Fig. 1). Alterations in miRNAs that target pro-calcific ligands such as BMP2 or signal intermediaries such as the SMADs may alter translational efficiency or destabilize mRNAs leading to changes in abundance. Consequently, we hypothesized that miRNA profiles differ in aorta from healthy control mice and *Klotho* homozygous mutant mice with renal disease. To identify miRNAs involved in aortic calcification, we profiled miRNAs in aortas from control healthy and *Klotho* mutant homozygotes. In total, 133 miRNAs were significantly increased, and 112 miRNAs were significantly decreased in *Klotho* mutant homozygous males relative to control mice ($p<0.05$, Fig. 3A, Table 1, Table S1, GSE135759). In *Klotho* mutant females, 96 miRNAs were significantly increased, and 58 miRNAs were significantly decreased ($p<0.05$, Fig. 3B, Table 1, Table S1, GSE135759). These results are consistent with a major role for miRNA-mediated post-transcriptional regulation in aortic calcification.

Differentially expressed miRNAs in Klotho mutant mice target osteogenic differentiation

We hypothesized that miRNAs that are differentially expressed in the calcified aortas of *Klotho* mutant mice may affect processes related to osteogenesis. In total, the abundance of 24 miRNAs was altered significantly in both male and female *Klotho* homozygous mutant mice relative to control mice ($p<0.05$, Fig. 3C, Table 2). Of these 9 miRNAs were up-regulated and 9 miRNAs were down-regulated in both sexes of *Klotho* homozygous mice. Table S2 lists genes predicted to be targeted by these 18 miRNAs that may directly influence BMP signaling without regard to sex.

Curiously, the abundances of 6 miRNAs were altered by *Klotho* homozygosity but in the opposite directions in each sex: miR-7019-5p, miR-3069-3p, miR-7685-3p and miR-679-5p were up-regulated in males and down-regulated in females, whereas miR-17-5p and miR-181c-3p were down-regulated in males and up-regulated in females (Table 2). The focus of this study was to restore natural repressive mechanisms whose weakening may contribute to pathological calcification. Therefore, we focused on miRNAs whose abundance is reduced in the calcified aorta of both sexes.

We used KEGG pathways and GO molecular function terms to computationally assign the potential roles of 9 down-regulated miRNAs. Similar analyses of all differentially regulated miRNAs in each sex are shown in Figures S1-4. These analyses revealed that signaling pathways involved in osteogenic differentiation: TGF-beta signaling (SMADs) pathways (6), MAPK, PI3K-Akt (31), HIPPO, WNT/beta-catenin and the AGE-RAGE signaling pathway in diabetic complications (32) were enriched among the predicted target genes (Fig. 4, Fig. S1-4). A manually compiled list of BMP signaling-relevant genes predicted by TargetScan to be targeted by selected miRNAs are shown in Table

S2. Together, these results suggest the disease-associated miRNA profile in *Klotho* homozygotes may influence the tendency of aortic cells to undergo osteogenic differentiation. We postulate that microRNAs that target more than one member of the BMP signaling pathway may inhibit BMP signaling by coordinately down-regulating multiple proteins and effectively restrain pathological calcification.

MicroRNA-145 and microRNA-378a attenuation in Klotho mutant mice

We selected two microRNAs to test the principle that a miRNA targeting several members of the BMP signaling pathway would reduce KLOTHO deficiency-associated calcification. The vascular regulator miR-145a is predicted to target *Bmp2*, *Smad1*, *5* and *9* (Fig. 5, Table S2, (33)), is down-regulated in the context of chronic kidney disease in an *ApoE* null background (34), and improves atherosclerotic symptoms in a mouse model of hyperlipidemia (35). Our microarray measurements showed that the abundance of miR-145a-5p was reduced by 20% in male *Klotho* homozygous mutant mice as compared to healthy control mice (Table S1). RT-PCR indicated that levels of both miR-145a-5p and -3p were significantly reduced in *Klotho* mutant mice of both sexes (Fig. 6A, B). The experiments described below test the impact of increasing miR-145 abundance in the setting of kidney failure and accelerated aging.

The abundance of another microRNA predicted to target both *Bmp2* and *Smad5*, miR-378a-5p, was sharply decreased in both male and female *Klotho* mutant mice (53% and 38% respectively, Table 2, Table S1). RT-PCR validated our microarray results and confirmed that the abundance of miR-378a-5p and -3p in *Klotho* mutant mice was half that present in healthy control aorta (Fig. 6C, D). Published reporter gene studies confirmed that miR-378 directly regulates *Bmp2* (36,37). Finally, the circulating level of miR-378 is reduced in the plasma of patients with coronary heart disease (1). Because predicted targeted sequences within the transcripts encoding BMP2 and SMAD proteins are conserved between mice and humans (Fig. 5), miR-145 and miR-378 are candidates for translational studies.

Forced overexpression of mir-145 and mir-378a in Klotho mutant mice

We used a vascular smooth muscle cell (VSMC)-specific *mSm22a* promoter-driven lentivirus to increase the abundance of miR-145 and miR-378a in the aortas of *Klotho* mutant homozygotes (Fig. 7A). To evaluate the efficacies and persistence of lentiviral transduction, RT-PCR was used to test the aortic levels of miR-145 and miR-378a in mice injected with viruses bearing these miRNAs relative to empty virus vectors. The miR-145 virus raised miR-145a-5p and miR-145a-3p abundances by 1.4±0.8 and 2.0±0.01 fold, respectively, relative to empty virus (Fig. 7B, C). Similarly, miR-378a-5p abundance increased by 1.7±0.04 fold (Fig. 7D) and miR-378a-3p abundance increased by 4.0±4.1 fold (Fig. 7E). Thus this delivery dosage and method successfully augmented aortic miR-145 and miR-378a levels in *Klotho* mutant mice.

Increased expression of miR-145 and miR-378a reduced BMP signaling and aortic calcification

Four different proteins involved in BMP signaling: *Bmp2, Smad1, 5 and 9* are

predicted to be targeted by miR-145 (Fig. 5, Table S2). Therefore, we hypothesized that increased miR-145 levels would repress the synthesis of these pro-osteogenesis factors and ameliorate pathological calcification. Having successfully augmented the level of miR-145 with lentivirus delivery, we evaluated the impact of this treatment on *Bmp2* and *Smad1, 5* and *9* RNA levels with RT-PCR. The *Bmp2* and *Smad5* RNA levels in aortas from mice injected with miR-145-bearing virus fell to 48±0.03% and 65±0.006% ($p < 0.05$) that of control aortas from mice injected with empty virus (Fig. 8A, C). The miR-145 virus did not significantly change the abundances of the *Smad1* (Fig. 8B) and *Smad9* (Fig. 8D).

To test if miR-145 overexpression inhibited pathological calcification in *Klotho* homozygous mutant mice, we compared the calcium present in the aortas of *Klotho* homozygous mutant mice injected with empty lentivirus vector or with virus bearing miR-145. The *Klotho* homozygous mutant mice injected with the miR-145 virus had one third less aortic calcium that in the empty virus injected mice (67±0.8%, $p = 0.002$, Fig. 8E). Thus, forced miR-145 expression limited pathological calcification in *Klotho* aorta.

The down-regulated miR-378a miRNA is predicted to target *Bmp2* and *Smad5* (Fig. 5, Table S2). To evaluate the potiential benefit of restoring miR-378a expression in the aorta of *Klotho* mutant mice, a lentivirus bearing miR-378a was injected. This virus reduced the levels of the target gene RNAs *Bmp2* and *Smad5* to 60±0.02% ($p = 0.02$) and 64±0.4% ($p = 0.04$) respectively of the RNA levels observed in the mice injected with empty virus (Fig. 9A and B). Finally, treatment with the mir-378a-bearing virus reduced aortic calcium levels by a third (63 ±0.6% of empty control, $p=0.02$) relative to levels in mice exposed to the empty virus (Fig. 9C). Thus as observed for miR-145, forced expression of miR-378a significantly ameliorated pathological calcification of the aorta.

Discussion

We obtained and analyzed miRNA profiles in aortas from control healthy and *Klotho* homozygous mutant mice with renal impairment that causes aortic calcification. Our KEGG pathway and GO molecular function term analyses of computationally predicted target genes suggest that many regulated miRNAs influence key signaling processes (Fig. 4, Fig. S1 - 4). Notably, in both sexes, pathways closely involved in osteogenic differentiation in bones and in pathological soft tissue calcification such as the BMP/TGF-beta and WNT/beta-catenin pathways were enriched. The target profiles are consistent with the prevailing view that cardiovascular calcification proceeds by known osteogenic mechanisms (4-7).

We recognize that a fraction of the miRNAs whose levels changed to a statistically significant level were regulated similarly in both male and female mice (Fig. 3C). This is partly explained by a limitation of our study whereby fewer female *Klotho* homozygotes were available (Table 3). The abundances of many miRNAs were changed in the same direction in both male and female mice, but the statistical significance of the change failed to reach our cutoff of $p<0.05$ in both sexes. However, the miRNA profiles between males and females also differ qualitatively. For example, the abundances of miR-17-5p, miR-181c-

3p, miR-7019-5p, miR-3069-3p, miR-7685-3p and miR-679-5p changed in opposite directions in males and females (Table 2). Interestingly, a class of miRNAs that modulate epithelial mesenchymal transition (miR-205 and the miR-200 family (38)) were highly up-regulated exclusively in female mice. MiR-205 and five members of the miR-200 family (miR-141, miR-200a, miR-429) were up-regulated by as much as 154-fold in *Klotho* mutant females but were unchanged in males (Table S1). Epithelial mesenchymal transition influences vascular calcification (39,40). Both quantitative and qualitative differences in aortic miRNA profiles in each sex may be highly clinically relevant because there are significant disparities in incidence, prognosis, and response to treatments for arterial diseases between men and women (41) We are separately investigating the sex-associated differences in the context of a study aimed at clarifying the impact of sex on BMP signaling (42).

We selected two miRNAs, miR-145 and miR-378, to test the principle that miRNAs targeting members of the BMP signaling pathway would reduce aortic calcification. We used the *Klotho* hypomorphic model because the swift pace of aortic calcification in the Klotho mutant homozygotes facilitates testing therapeutic approaches to reducing calcification. In contrast, other models are experimentally time-consuming. For example, mice with genetically sensitized hyperlipidemia backgrounds must be fed special diets for months (43,44). In *Klotho* mutant mice with hyperphosphatemia elevated aortic BMP signaling and calcification is observed at 6-7 weeks of age (Fig. 1, (19,45). In this model, only 10 days of exposure to viruses overexpressing miR-145 and miR-378 limited pathological calcification (Fig. 8,9). Studies using *Klotho* mice with renal disease also are relevant to human biology, because KLOTHO deficiency is associated with chronic kidney disease that promotes valve and vascular calcification in people (46-49). This work underscores the great potential for miRNA-based therapies in treating calcification pathologies.

Restoration of aortic miR-145 levels has also been shown to decrease atherosclerotic plaque size, increase plaque stability, and promote a contractile cell phenotype in the ApoE, high fat diet mouse model of hyperlipidemia (35). Our demonstration of reduced calcification in *Klotho* mutant homozygous mice with forced miR-145 (Fig. 8) indicates that miR-145 can attenuate vascular disease in a model of atherosclerosis caused by hyperphosphatemia. The effectiveness of this microRNA in these highly dissimilar physiological situations suggest that miR-145 directly promotes vascular health and inhibits pathological osteogenesis.

Like miR-145, miR-378a was significantly down-regulated in blood samples from patients with coronary artery disease compared to healthy subjects (50). Furthermore, both miRNAs target regions of the BMP2 and other BMP signaling genes that are highly conserved between mice and humans (Fig. 5). Interestingly, both miRNAs are subject to editing whereby specific adenosines are post-transcriptionally converted to inosine (51,52). Inosine base pairs cytosine, not thymine. Manual sequence inspection indicates that editing would increase the complementarity of miR-145 and miR-378a for sites within both the mouse and

human *BMP2* messages. Although editing may significantly change miRNA/message interactions, current databases and prediction tools do not facilitate global predictions of how edited miRNAs may impact signaling pathways.

In summary, we have provided a database of the miRNAs that are differentially expressed in healthy mouse aorta relative to aorta calcified due to defective mineral metabolism and kidney function. We also demonstrated that forced expression of miR-145 and miR-378 inhibited RNAs encoding BMP signaling proteins and chronic kidney disease-associated aortic calcification. MiRNA-145 and miR-378 are candidates for translational studies investigating therapies to block vascular calcification.

Experimental procedures

Tissue collection

Mice bearing the *Klotho* mutation were a gracious gift from Dr. Makoto Kuro-o (Jichi Medical University) by way of Dr. Sylvia Christakos (Rutgers New Jersey Medical School). The mice were a mixture of strains FVB, C57Bl/6J, and C3H/J. Because homozygous *Klotho* null mice are infertile, mice were maintained by heterozygous-by-heterozygous mating. 25% of each litter was homozygous and exhibited the full *Klotho* phenotype, including ectopic soft tissue calcification. 50% were heterozygous and 25% were wild type. No statistically significant differences in any parameter were observed between mice bearing the heterozygous and wild type *Klotho* genotypes. Assessed parameters included body and organ weights, gene expression, and calcium levels (Table S4). Because our analyses were consistent with published data indicating that the *Klotho* mutation is fully recessive, heterozygous and wild type samples were presented together as “healthy control” samples.

All animal procedures were in accordance with the guidelines for Care and Use of Experimental Animals and approved by the NJ Medical School Institutional Animal Care and Use Committee (IACUC protocol #PROTO999900898). Control and *Klotho* homozygote mice were fed regular chow and euthanized at 50 $\pm$ 1 days of age. After weaning, *Klotho* homozygotes received softened chow on the floor of the cage. On the day of necropsy, mice were killed with an inhalation overdose of isoflurane. Immediately thereafter, the heart was perfused *via* the left ventricle with phosphate buffered saline (PBS, pH 7.3), to remove excess blood. The aorta including the ascending aorta, arch and descending thoracic aorta was removed. After cutting at the surface of the heart, the aorta was rinsed in PBS, blot dried and weighed. The aorta was snap-frozen in liquid nitrogen and stored at -80°C. Frozen tissues were ground in liquid nitrogen using a mortar and pestle. To facilitate handling small tissues such as the diseased aortas from *Klotho* homozygotes, acid-washed glass beads (Millipore-SIGMA, St. Louis, MO, # G1277) were added during the grinding. Glass beads did not affect the biochemical assays (Fig. S7A, B).

Western Blots

Frozen ground tissue was solubilized in RIPA buffer, sonicated, and subjected to western blot analyses as described in Shah et al (26). BMP signaling was measured using a monoclonal phospho-SMAD 1/5/9(8) antibody (Cell Signaling Technology, Danvers, MA, #13820) at a

dilution of 1:1000. The pSMAD antibody was authenticated as described in Fig. S7C and D. Polyclonal total SMAD 1/5/9(8) (Santa Cruz Biotechnology, Inc., Santa Cruz, CA, #sc-6031-R) and a polyclonal actin antibody (Santa Cruz Biotechnology, Inc., Santa Cruz, CA, #sc-1615-R) were subsequently used at a dilution of 1:1000. In all cases, the secondary antibody was Goat Anti-Rabbit HRP (Abcam, Cambridge, MA, # ab97080) at a dilution of 1: 20,000. Antibody-bound proteins were detected using SuperSignal™ West Femto Maximum Sensitivity Substrate (ThermoFisher Scientific, Waltham, MA, # 34096) and imaged using a FluoroChem M (Protein Simple, San Jose, California).

Calcium assays

Ground tissue was solubilized and lysed by sonication on ice in PBS, pH 7.3 containing 0.16 mg/mL heparin. The Cayman Chemical Calcium Assay kit was used to measure calcium levels (Ann-Arbor, MI, #701220). Calcium levels were normalized to protein levels measured using the Bradford assay (Bio-Rad Laboratories, Hercules, CA, # 5000006).

Spatial mapping of calcified structures

The patterns of mineralization in *Klotho* heterozygote *vs. Klotho* mutant mice were determined using microcomputerized tomography (microCT) at the Rutgers Molecular Imaging Center (http://imaging.rutgers.edu/). Mice were scanned using the Albira® PET/CT (Carestream, Rochester, NY) at standard voltage and current settings (45kV and 400μA) with a minimal voxel size of <35 μm. Voxel intensities in the reconstructed images were evaluated and segmented with VivoQuant image analysis software (version 1.23, inviCRO LLC, Boston).

MicroRNA microarray and data analysis

Aortic samples were obtained from both male and female control and *Klotho* mutant mice at 7 to 8 weeks of age (Table 3). RNA was extracted using the miRNeasy Mini Kit (Qiagen Inc., Germantown, MD, # 217004). The RNA quality was checked using a Bioanalyzer (Agilent Technologies, Santa Clara, CA).

MicroRNA expression in the aorta was assessed with the Applied Biosystems™ GeneChip™ miRNA 4.0 Array (ThermoFisher Scientific, Waltham, MA, #902412) in the Rutgers NJMS Genomics Center. The GeneChip™ miRNA 4.0 Array contained the miRNAs and pre-miRNAs (precursors to the miRNAs) listed in the Sanger miRBase v20. The miRNA arrays were processed following the manufacturer's instructions. Briefly, using the Applied Biosystems™ FlashTag™ Biotin HSR RNA Labeling Kit (ThermoFisher Scientific, Waltham, MA, the # 902446), 400 ng of total RNA was labeled with biotin and hybridized to the miRNA 4.0 Array (ThermoFisher Scientific, Waltham, MA, #902412) for 18 hours at 48°C using an Affymetrix® 450 Hybridization Oven (Affymetrix, Santa Clara, CA). After washing and staining on an Affymetrix® 450 Fluidics Station (Affymetrix, Santa Clara, CA), using the Applied Biosystems™ GeneChip™ Hybridization, Wash, and Stain Kit (ThermoFisher Scientific, Waltham, MA, #900720), the arrays were scanned using the Affymetrix® Scanner 3000 7G (Affymetrix, Santa Clara, CA). CEL files were generated using the Affymetrix

data extraction protocol in the Affymetrix GeneChip® Command Console® Software (Affymetrix, Santa Clara, CA, USA). The resulting CEL files (GSE135759) were analyzed using the Transcriptome Analysis Console 4.0 (TAC, ThermoFisher Scientific, Waltham, MA), including the Robust-Multi-array Average algorithm to correct for microarray background and to normalize miRNA expression profiles on a log scale. TAC's ANOVA analysis identified the miRNAs whose abundance differed significantly between control and *Klotho* homozygous mutant mice. Minimal significance was defined as a *p* value of 0.05.

Bioinformatic analyses

MicroRNAs that significantly down-regulated in both sexes of *Klotho* homozygous mice compared to control were further used to perform target prediction (see microarray data analysis). Predicted target profiles were obtained from the DNA Intelligent Analysis (DIANA)-micro T-CDS (v. 5.0) which permits the entry of multiple miRNAs simultaneously (http://www.microrna.gr/webServer) (53). The micro T-CDS threshold score for predicted targets was set at 0.6. Scores ranged from 0 to 1, with a higher score indicating an increased probability of a true microRNA target. To classify and visualize the biological processes affected by the target genes predicted by DIANA, Gene Ontology (GO) and KEGG (Kyoto Encyclopedia of Genes and Genomes) were utilized with the R package, clusterProfiler (http://bioconductor.org/packages/release/bioc/html/clusterProfiler.html) (54). Minimal significance was defined as a *p* value of 0.05. Alignments between selected miRNAs and mouse genes were predicted by MiRanda (55) and TargetScan 7.2 (http://www.targetscan.org/mmu_72/ (56)).

Real-Time Reverse Transcription PCR for detection of microRNA-145 and microRNA-378a and target gene expression

MicroRNA cDNA was synthesized using the miScript PCR Kit (Qiagen Inc., Germantown, MD, # 218073). The miScript PCR kit utilized a universal oligo-dT primer tag to convert all RNA species (total RNA and miRNA) into cDNA. A universal reverse primer supplied with the miScript PCR kit was used to amplify cDNA from each miRNA. The miRNA forward primers were designed based on miRNA sequences in miRBase 22 (http://www.mirbase.org/). GCG or CGC was added to the 5' end of the primers when the GC % was low. NCBI nucleotide blast was used to confirm the absence of non-specific binding sites for the forward primers. Messenger RNA (mRNA) cDNA was synthesized using the QuantiTect® Reverse Transcription kit (Qiagen Inc., Germantown, MD, # 205313). Intron-spanning primers for mRNA were used to eliminate amplicons generated from any contaminating genomic DNA. Primer sequences are shown in Table 4.

Quantitative PCR was performed on a CFX96 Touch™ Real-Time PCR Detection System (Bio-Rad Laboratories, Hercules, CA, #1855196) using the QuantiTect® SYBR® Green PCR kit (Qiagen Inc., Germantown, MD, #204145) under the following conditions: 15 min at 95°C, 39 cycles of 15 seconds at 94°C, 30 seconds at 55°C and 30 seconds 70°C. MicroRNA abundance was normalized to U6 and mRNA

expression was normalized to actin. The human U6 primer used in this experiment was included in the miScript Primer assay kit (Qiagen Inc., Germantown, MD, #218300).

Lentiviral microRNA-145 and microRNA-378a transduction

A lentivirus vector expressing mir-145 or mir-378a under the control of the vascular smooth muscle cell (VSMC)-specific mSm22a promoter was purchased from Biosettia (Biosettia Inc, San Diego, CA). The negative control was the empty virus vector. Newly weaned *Klotho* mutant homozygotes were injected with empty lentivirus or lentivirus bearing mir-145 or mir-378a *via* their tail veins on 5 alternate days. The total lentivirus achieved in each mouse at the end of the treatment window was 4×10^5 pfu/g body weight. The mir-145 lentivirus generates two mature miRNAs: miR-145a-5p and miR-145a-3p. The mir-378a lentivirus generates two mature miRNAs: miR-378a-5p and miR-378a-3p.

Statistical Analysis

Data are presented as mean ± SEM and analyzed with GraphPad (version 7; GraphPad Software Inc, La Jolla, CA). Statistical significance was assessed with either the Student's two-tailed t-test or one-way ANOVA. Differences were considered significant if $p<0.05$.

Acknowledgements: We warmly thank Youhua Zhu for her diligent technical assistance, Dr. Diane Garsetti for critically reading the manuscript, and Lindsey Zhu for bioinformatics assistance. We appreciate the technical assistance provided by the NJMS Genomics Center.

Conflict of Interests statement: The authors declare that they have no conflicts of interest with the contents of this article.

References

1. Benjamin, E. J., Muntner, P., Alonso, A., Bittencourt, M. S., Callaway, C. W., Carson, A. P., Chamberlain, A. M., Chang, A. R., Cheng, S., Das, S. R., Delling, F. N., Djousse, L., Elkind, M. S. V., Ferguson, J. F., Fornage, M., Jordan, L. C., Khan, S. S., Kissela, B. M., Knutson, K. L., Kwan, T. W., Lackland, D. T., Lewis, T. T., Lichtman, J. H., Longenecker, C. T., Loop, M. S., Lutsey, P. L., Martin, S. S., Matsushita, K., Moran, A. E., Mussolino, M. E., O'Flaherty, M., Pandey, A., Perak, A. M., Rosamond, W. D., Roth, G. A., Sampson, U. K. A., Satou, G. M., Schroeder, E. B., Shah, S. H., Spartano, N. L., Stokes, A., Tirschwell, D. L., Tsao, C. W., Turakhia, M. P., VanWagner, L. B., Wilkins, J. T., Wong, S. S., Virani, S. S., American Heart Association Council on, E., Prevention Statistics, C., and Stroke Statistics, S. (2019) Heart Disease and Stroke Statistics-2019 Update: A Report From the American Heart Association. *Circulation* **139**, e56-e528
2. Karwowski, W., Naumnik, B., Szczepanski, M., and Mysliwiec, M. (2012) The mechanism of vascular calcification - a systematic review. *Med Sci Monit* **18**, RA1-11
3. Yutzey, K. E., Demer, L. L., Body, S. C., Huggins, G. S., Towler, D. A., Giachelli, C. M., Hofmann-Bowman, M. A., Mortlock, D. P., Rogers, M. B., Sadeghi, M. M., and Aikawa, E. (2014) Calcific aortic valve disease: a consensus summary from the Alliance of Investigators on Calcific Aortic Valve Disease. *Arterioscler Thromb Vasc Biol* **34**, 2387-2393
4. Towler, D. A. (2017) Commonalities Between Vasculature and Bone An Osseocentric View of Arteriosclerosis. *Circulation* **135**, 320-322
5. Bostrom, K. I., Rajamannan, N. M., and Towler, D. A. (2011) The regulation of valvular and vascular sclerosis by osteogenic morphogens. *Circ Res* **109**, 564-577
6. Garcia de Vinuesa, A., Abdelilah-Seyfried, S., Knaus, P., Zwijsen, A., and Bailly, S. (2016) BMP signaling in vascular biology and dysfunction. *Cytokine Growth Factor Rev* **27**, 65-79
7. Leopold, J. A. (2012) Cellular mechanisms of aortic valve calcification. *Circ Cardiovasc Interv* **5**, 605-614
8. Bostrom, K., Watson, K. E., Horn, S., Wortham, C., Herman, I. M., and Demer, L. L. (1993) Bone morphogenetic protein expression in human atherosclerotic lesions. *J Clin Invest* **91**, 1800-1809
9. Nagy, E., Eriksson, P., Yousry, M., Caidahl, K., Ingelsson, E., Hansson, G. K., Franco-Cereceda, A., and Back, M. (2013) Valvular osteoclasts in calcification and aortic valve stenosis severity. *Int J Cardiol* **168**, 2264-2271
10. Yang, X., Meng, X., Su, X., Mauchley, D. C., Ao, L., Cleveland, J. C., Jr., and Fullerton, D. A. (2009) Bone morphogenic protein 2 induces Runx2 and osteopontin expression in human aortic valve interstitial cells: role of Smad1 and extracellular signal-regulated kinase 1/2. *J Thorac Cardiovasc Surg* **138**, 1008-1015
11. Cheng, S. L., Shao, J. S., Charlton-Kachigian, N., Loewy, A. P., and Towler, D. A. (2003) MSX2 promotes osteogenesis and suppresses adipogenic

differentiation of multipotent mesenchymal progenitors. *J Biol Chem* **278**, 45969-45977

12. Yu, Z., Seya, K., Daitoku, K., Motomura, S., Fukuda, I., and Furukawa, K. (2011) Tumor necrosis factor-alpha accelerates the calcification of human aortic valve interstitial cells obtained from patients with calcific aortic valve stenosis via the BMP2-Dlx5 pathway. *J Pharmacol Exp Ther* **337**, 16-23
13. Osman, L., Yacoub, M. H., Latif, N., Amrani, M., and Chester, A. H. (2006) Role of human valve interstitial cells in valve calcification and their response to atorvastatin. *Circulation* **114**, I547-552
14. Nigam, V., and Srivastava, D. (2009) Notch1 represses osteogenic pathways in aortic valve cells. *J Mol Cell Cardiol* **47**, 828-834
15. Wirrig, E. E., Hinton, R. B., and Yutzey, K. E. (2011) Differential expression of cartilage and bone-related proteins in pediatric and adult diseased aortic valves. *J Mol Cell Cardiol* **50**, 561-569
16. Miller, J. D., Weiss, R. M., Serrano, K. M., Castaneda, L. E., Brooks, R. M., Zimmerman, K., and Heistad, D. D. (2010) Evidence for active regulation of pro-osteogenic signaling in advanced aortic valve disease. *Arterioscler Thromb Vasc Biol* **30**, 2482-2486
17. Mohler, E. R., 3rd, Gannon, F., Reynolds, C., Zimmerman, R., Keane, M. G., and Kaplan, F. S. (2001) Bone formation and inflammation in cardiac valves. *Circulation* **103**, 1522-1528
18. Nakagawa, Y., Ikeda, K., Akakabe, Y., Koide, M., Uraoka, M., Yutaka, K. T., Kurimoto-Nakano, R., Takahashi, T., Matoba, S., Yamada, H., Okigaki, M., and Matsubara, H. (2010) Paracrine osteogenic signals via bone morphogenetic protein-2 accelerate the atherosclerotic intimal calcification in vivo. *Arterioscler Thromb Vasc Biol* **30**, 1908-1915
19. Gomez-Stallons, M. V., Wirrig-Schwendeman, E. E., Hassel, K. R., Conway, S. J., and Yutzey, K. E. (2016) Bone Morphogenetic Protein Signaling Is Required for Aortic Valve Calcification. *Arterioscler Thromb Vasc Biol* **36**, 1398-1405
20. Balachandran, K., Sucosky, P., Jo, H., and Yoganathan, A. P. (2010) Elevated cyclic stretch induces aortic valve calcification in a bone morphogenic protein-dependent manner. *Am J Pathol* **177**, 49-57
21. Derwall, M., Malhotra, R., Lai, C. S., Beppu, Y., Aikawa, E., Seehra, J. S., Zapol, W. M., Bloch, K. D., and Yu, P. B. (2012) Inhibition of bone morphogenetic protein signaling reduces vascular calcification and atherosclerosis. *Arterioscler Thromb Vasc Biol* **32**, 613-622
22. Malhotra, R., Burke, M. F., Martyn, T., Shakartzi, H. R., Thayer, T. E., O'Rourke, C., Li, P., Derwall, M., Spagnolli, E., Kolodziej, S. A., Hoeft, K., Mayeur, C., Jiramongkolchai, P., Kumar, R., Buys, E. S., Yu, P. B., Bloch, K. D., and Bloch, D. B. (2015) Inhibition of bone morphogenetic protein signal transduction prevents the medial vascular calcification associated with matrix Gla protein deficiency. *PLoS One* **10**, e0117098
23. Corbett, A. H. (2018) Post-transcriptional regulation of gene expression and human disease. *Curr Opin Cell Biol* **52**, 96-104

24. Fotinos, A., Fritz, D. T., Lisica, S., Liu, Y., and Rogers, M. B. (2016) Competing Repressive Factors Control Bone Morphogenetic Protein 2 (BMP2) in Mesenchymal Cells. *J Cell Biochem* **117**, 439-447
25. Rogers, M. B., Shah, T. A., and Shaikh, N. N. (2015) Turning Bone Morphogenetic Protein 2 (BMP2) on and off in Mesenchymal Cells. *J Cell Biochem* **116**, 2127-2138
26. Shah, T. A., Zhu, Y., Shaikh, N. N., Harris, M. A., Harris, S. E., and Rogers, M. B. (2017) Characterization of new bone morphogenetic protein (Bmp)-2 regulatory alleles. *Genesis* **55**, 10.1002/dvg.23035
27. Johnson, J. L. (2019) Elucidating the contributory role of microRNA to cardiovascular diseases (a review). *Vascul Pharmacol* **114**, 31-48
28. Kuro-o, M., Matsumura, Y., Aizawa, H., Kawaguchi, H., Suga, T., Utsugi, T., Ohyama, Y., Kurabayashi, M., Kaname, T., Kume, E., Iwasaki, H., Iida, A., Shiraki-Iida, T., Nishikawa, S., Nagai, R., and Nabeshima, Y. I. (1997) Mutation of the mouse klotho gene leads to a syndrome resembling ageing. *Nature* **390**, 45-51
29. Hu, M. C., Shi, M., Zhang, J., Quinones, H., Griffith, C., Kuro-o, M., and Moe, O. W. (2011) Klotho deficiency causes vascular calcification in chronic kidney disease. *J Am Soc Nephrol* **22**, 124-136
30. Yamada, S., and Giachelli, C. M. (2017) Vascular calcification in CKD-MBD: Roles for phosphate, FGF23, and Klotho. *Bone* **100**, 87-93
31. Guntur, A. R., and Rosen, C. J. (2011) The skeleton: a multi-functional complex organ. New insights into osteoblasts and their role in bone formation: the central role of PI3Kinase. *Journal of Endocrinology* **211**, 123-130
32. Kay, A. M., Simpson, C. L., and Stewart, J. A., Jr. (2016) The Role of AGE/RAGE Signaling in Diabetes-Mediated Vascular Calcification. *J Diabetes Res* **2016**, 10.1155/2016/6809703
33. Vacante, F., Denby, L., Sluimer, J. C., and Baker, A. H. (2019) The function of miR-143, miR-145 and the MiR-143 host gene in cardiovascular development and disease. *Vascul Pharmacol* **112**, 24-30
34. Taibi, F., Metzinger-Le Meuth, V., M'Baya-Moutoula, E., Djelouat, M., Louvet, L., Bugnicourt, J. M., Poirot, S., Bengrine, A., Chillon, J. M., Massy, Z. A., and Metzinger, L. (2014) Possible involvement of microRNAs in vascular damage in experimental chronic kidney disease. *Biochim Biophys Acta* **1842**, 88-98
35. Lovren, F., Pan, Y., Quan, A., Singh, K. K., Shukla, P. C., Gupta, N., Steer, B. M., Ingram, A. J., Gupta, M., Al-Omran, M., Teoh, H., Marsden, P. A., and Verma, S. (2012) MicroRNA-145 targeted therapy reduces atherosclerosis. *Circulation* **126**, S81-90
36. Yang, Y. J., Luo, S., and Wang, L. S. (2019) Effects of microRNA-378 on epithelial-mesenchymal transition, migration, invasion and prognosis in gastric carcinoma by targeting BMP2. *Eur Rev Med Pharmacol Sci* **23**, 5176-5186
37. Hou, X., Tang, Z., Liu, H., Wang, N., Ju, H., and Li, K. (2012) Discovery of MicroRNAs associated with myogenesis by deep sequencing of serial developmental skeletal muscles in pigs. *PLoS One* **7**, e52123
38. Samavarchi-Tehrani, P., Golipour, A., David, L., Sung, H. K., Beyer, T. A., Datti, A., Woltjen, K., Nagy, A., and Wrana, J. L. (2010) Functional genomics reveals a

BMP-driven mesenchymal-to-epithelial transition in the initiation of somatic cell reprogramming. *Cell Stem Cell* **7**, 64-77

39. Bostrom, K. I., Yao, J., Guihard, P. J., Blazquez-Medela, A. M., and Yao, Y. (2016) Endothelial-mesenchymal transition in atherosclerotic lesion calcification. *Atherosclerosis* **253**, 124-127
40. Sanchez-Duffhues, G., Garcia de Vinuesa, A., van de Pol, V., Geerts, M. E., de Vries, M. R., Janson, S. G., van Dam, H., Lindeman, J. H., Goumans, M. J., and Ten Dijke, P. (2019) Inflammation induces endothelial-to-mesenchymal transition and promotes vascular calcification through downregulation of BMPR2. *J Pathol* **247**, 333-346
41. den Ruijter, H. M., Haitjema, S., Asselbergs, F. W., and Pasterkamp, G. (2015) Sex matters to the heart: A special issue dedicated to the impact of sex related differences of cardiovascular diseases. *Atherosclerosis* **241**, 205-207
42. Shah, T. A. (2018) *Post-transcriptional Gene Regulation of Bone Morphogenetic Protein (BMP)-2 During Embryogenesis and Cardiovascular Calcification.* Ph.D., Rutgers School of Graduate Studies
43. Neven, E., and D'Haese, P. C. (2011) Vascular calcification in chronic renal failure: what have we learned from animal studies? *Circ Res* **108**, 249-264
44. Miller, J. D., Weiss, R. M., and Heistad, D. D. (2011) Calcific aortic valve stenosis: methods, models, and mechanisms. *Circ Res* **108**, 1392-1412
45. Tapan A. Shah, Y. T., Edward J. Yurkow, Melissa B. Rogers. (2019) Post-Transcriptional Bone Morphogenetic Protein 2 (BMP2) Gene Regulation 1 in Aorta. *biorxiv=735852*
46. Koh, N., Fujimori, T., Nishiguchi, S., Tamori, A., Shiomi, S., Nakatani, T., Sugimura, K., Kishimoto, T., Kinoshita, S., Kuroki, T., and Nabeshima, Y. (2001) Severely reduced production of klotho in human chronic renal failure kidney. *Biochem Biophys Res Commun* **280**, 1015-1020
47. Ichikawa, S., Imel, E. A., Kreiter, M. L., Yu, X., Mackenzie, D. S., Sorenson, A. H., Goetz, R., Mohammadi, M., White, K. E., and Econs, M. J. (2007) A homozygous missense mutation in human KLOTHO causes severe tumoral calcinosis. *J Clin Invest* **117**, 2684-2691
48. Arking, D. E., Atzmon, G., Arking, A., Barzilai, N., and Dietz, H. C. (2005) Association between a functional variant of the KLOTHO gene and high-density lipoprotein cholesterol, blood pressure, stroke, and longevity. *Circ Res* **96**, 412-418
49. Arking, D. E., Becker, D. M., Yanek, L. R., Fallin, D., Judge, D. P., Moy, T. F., Becker, L. C., and Dietz, H. C. (2003) KLOTHO allele status and the risk of early-onset occult coronary artery disease. *Am J Hum Genet* **72**, 1154-1161
50. Weber, M., Baker, M. B., Patel, R. S., Quyyumi, A. A., Bao, G., and Searles, C. D. (2011) MicroRNA Expression Profile in CAD Patients and the Impact of ACEI/ARB. *Cardiol Res Pract* **2011**, 532915
51. Shoshan, E., Mobley, A. K., Braeuer, R. R., Kamiya, T., Huang, L., Vasquez, M. E., Salameh, A., Lee, H. J., Kim, S. J., Ivan, C., Velazquez-Torres, G., Nip, K. M., Zhu, K., Brooks, D., Jones, S. J., Birol, I., Mosqueda, M., Wen, Y. Y., Eterovic, A. K., Sood, A. K., Hwu, P., Gershenwald, J. E., Robertson, A. G., Calin, G. A., Markel, G., Fidler, I. J., and Bar-Eli, M. (2015) Reduced adenosine-to-inosine

miR-455-5p editing promotes melanoma growth and metastasis. *Nat Cell Biol* **17**, 311-321

52. Zheng, Y., Li, T., Ren, R., Shi, D., and Wang, S. (2014) Revealing editing and SNPs of microRNAs in colon tissues by analyzing high-throughput sequencing profiles of small RNAs. *BMC Genomics* **15 Suppl 9**, S11
53. Paraskevopoulou, M. D., Georgakilas, G., Kostoulas, N., Vlachos, I. S., Vergoulis, T., Reczko, M., Filippidis, C., Dalamagas, T., and Hatzigeorgiou, A. G. (2013) DIANA-microT web server v5.0: service integration into miRNA functional analysis workflows. *Nucleic Acids Res* **41**, W169-173
54. Yu, G., Wang, L. G., Han, Y., and He, Q. Y. (2012) clusterProfiler: an R package for comparing biological themes among gene clusters. *OMICS* **16**, 284-287
55. Betel, D., Wilson, M., Gabow, A., Marks, D. S., and Sander, C. (2008) The microRNA.org resource: targets and expression. *Nucleic Acids Research* **36**, D149-D153
56. Agarwal, V., Bell, G. W., Nam, J. W., and Bartel, D. P. (2015) Predicting effective microRNA target sites in mammalian mRNAs. *Elife* **4**, 10.7554/eLife.05005

Table 1. The number and percentage of miRNAs that differed in control relative to *Klotho* homozygotes (KK), p<0.05

	Male	**Female**
Any significant change		
Increased in KK	133 (7.0%)	100 (5.2%)
Reduced in KK	113 (5.9%)	58 (3.0%)
1.5-fold difference		
Increased in KK	88 (4.6%)	70 (3.7%)
Reduced in KK	62 (3.2%)	34 (1.8%)
2-fold difference		
Increased in KK	57 (3.0%)	46 (2.4%)
Reduced in KK	30 (1.6%)	20 (1.0%)

Table 2. Relative abundance of miRNAs that were differentially expressed in both male and female *Klotho* homozygous mutant mice

Name	% control in males (p value)	% control in females (p value)
miR-16-1-3p	1,344 (0.0001)	1,331 (0.04)
miR-466f-5p	489 (0.001)	540 (0.03)
miR-669k-5p	415 (0.00007)	331 (0.01)
miR-7684-3p	185 (0.002)	231 (0.003)
miR-744-5p	171 (0.0001)	294 (0.00008)
miR-1930-3p	156 (0.01)	312 (0.005)
miR-383-5p	137 (0.02)	215 (0.02)
miR-6929-3p	127 (0.01)	167 (0.02)
miR-7080-3p	114 (0.03)	145 (0.03)
miR-7019-5p	156 (0.03)	63 (0.045)
miR-3069-3p	143 (0.02)	55 (0.04)
miR-7685-3p	121 (0.002)	85 (0.04)
miR-679-5p	113 (0.007)	86 (0.046)
miR-17-5p	78 (0.02)	205 (0.03)
miR-181c-3p	42 (0.02)	263 (0.02)
miR-187-5p	84 (0.01)	55 (0.02)
miR-330-3p	67 (0.01)	41 (0.02)
miR-187-3p	65 (0.009)	29 (0.009)
miR-378c	63 (0.03)	47 (0.002)
miR-193a-3p	55 (0.0003)	34 (0.0004)
miR-378a-5p	53 (0.00009)	38 (0.0004)
miR-365-1-5p	51 (0.04)	41 (0.02)
miR-193b-5p	46 (0.02)	15 (0.0003)
miR-193b-3p	45 (0.00003)	30 (0.00003)

Table 3. Number of mice (n) used for the miRNA profiling

	Males	**Females**
Group	**n**	**n**
Control (Wt)	5	4
Control (K+)	2	1
Klotho mutant (KK)	5	2

Table 4. Reverse Transcription PCR primer sequences

Name	**Primer Sequence (5'-3')**
mmu-miR-145a-3p	F: GCGATTCCTGGAAATACTGTTCTTG
mmu-miR-145a-5p	F: GTCCAGTTTTCCCAGGAATCCCT
mmu-miR-378a-5p	F: CTCCTGACTCCAGGTCCTGTGT
mmu-miR-378a-3p	F: ACTGGACTTGGAGTCAGAAGG
Mouse *Bmp2*	F: TAGATCTGTACCGCAGGCA R: GTTCCTCCACGGCTTCTTC
Mouse *Smad1*	F: GTGTATGAACTCACCAAAATGTGC R: TAACATCCTGCCGGTGGTATTC
Mouse *Smad5*	F: AACTTTCACCATGGCTTCCA R: CCAGAAGCTGAGCAAACTCC
Mouse *Smad9*	F: CGATCATTCCATGAAGCTGACAA R: TGGGCAAGCCAAACCGATA
Mouse *β-actin*	F: CGCCACCAGTTCGCCATGGA R: TACAGCCCGGGGAGCATCGT

FOOTNOTES

Funding was provided by grants from the National Heart, Lung, and Blood Institute (R01HL114751) and National Institutes of Aging (R56AG050762) and from the NJMS Research Core Facilities Matching Funds Small Grants Program to MBR and an American Heart Association fellowship (20POST35210235) to YT.

The abbreviations used are: BMP2: bone morphogenetic protein 2; miRNAs: microRNAs; mRNA: messenger RNA; BMPR: BMP receptor; 3'-UTR: 3'-untranslated region; VSMC: vascular smooth muscle cell; GO: Gene Ontology; KEGG: Kyoto Encyclopedia of Genes and Genomes; NJMS, New Jersey Medical School

Fig. 1. BMP signaling and calcification levels in aorta from homozygous *Klotho* mutant mice. Aortas were isolated from control (C) mice with normal kidney function ($Kl^{+/+}$ and $Kl^{kl/+}$) or mice homozygous ($Kl^{kl/kl}$) for the *Klotho* mutation with renal disease (KK) between 40 and 50 days of age. Average parameter values are presented with standard error measurements (SEM). **A.** BMP signaling levels as assessed by phosphorylated SMAD1/5/9 (pSMAD) levels normalized to total SMAD1/5/9 (tSMAD) (males, n = 3 – 6; females, n = 5 – 7). **B.** Representative western blot panels showing pSMAD1/5/9 and total SMAD1/5/9 levels, males (top) and females (bottom). **C.** Average calcium levels normalized to protein concentration (males, n = 9 – 18; females, n = 6 – 7). All experiments were repeated at least twice with similar results. * $p < 0.05$, **** $p < 0.001$. **D, E.** Male littermates *w*ere scanned with an Albira PET/CT Imaging System (Carestream, Rochester, NY) set at 45 kV, 400 µA, and <35 µm voxel size. Voxel intensities in the reconstructed images were evaluated and segmented with VivoQuant image analysis software (version 1.23, inviCRO LLC, Boston MA). The dashed white lines mark mineralized areas of the aortic sinus and ascending aorta present in the heart (**Ht**) of the *Klotho* mutant homozygote **(E)**, but not in the heterozygous control $Kl^{kl/+}$ **(D)**.

Fig. 2. *Bmp2* and *Smad1, 5,* and *9* mRNA abundances in aorta from control and homozygous *Klotho* mutant mice. Aortas were isolated from control mice bearing the wild type (Wt) or heterozygous (+/*Kl*) *Klotho* genotypes, or diseased (KK) homozygous ($Kl^{kl/kl}$) *Klotho* mice between 40 and 50 days of age. *Klotho* mutant homozygous mice had pathologically calcified aorta. *Bmp2* **(A)** and *Smad1* **(B)** RNA levels did not change. *Smad5* **(C)** and *9* **(D)** RNA levels were significantly increased relative to control mice. The bars indicate the mean value +/- SEM. Solid and hollow circles represent individual male and female values, respectively. * = $p < 0.05$, ** = $p < 0.01$.

Fig. 3. MicroRNA profiles in the aorta from control and *Klotho homozygous (KK)* mutant mice. RNA was extracted from the aorta of healthy controls ($Kl^{+/+}$ and $Kl^{kl/+}$) or *Klotho* homozygous ($Kl^{kl/kl}$) mice (KK). Samples were assayed using Affymetrix miRNA version 4.0. Data analysis was performed after Robust Multi-Array Average (RMA) normalization with Transcriptome Analysis Console (TAC). **A, B.** Volcano plots illustrate miRNAs whose abundances differed significantly in aorta from diseased mice compared to control mice ($p < 0.05$). The X axis indicates $\log_2$ fold change and the Y axis indicates $-\log_{10}$ p value. Vertical dotted lines indicate 2-fold change. **C.** The Venn diagram shows the number and percentage of miRNAs differentially expressed in male or female mice or in both out of 1908 miRNAs.

Fig. 4. Gene Ontology (GO) and KEGG (Kyoto Encyclopedia of Genes and Genomes) analyses of miRNAs down-regulated in both sexes of *Klotho* homozygous mutant mice. The genes potentially targeted by down-regulated miRNAs

were predicted by DIANA TOOLS. **A.** Target genes were grouped into gene pathways using the KEGG database. The y-axis represents the name of the KEGG pathway, and the x-axis represents the number of the genes in a certain pathway. **B.** Target genes were grouped into GO molecular function terms using the GO database. The y-axis represents the name of the GO molecular function term, and the x-axis represents the number of genes associated with each GO molecular function term. Low p adjust values are in red and high p adjust values are in blue. GO terms and KEGG pathways that are directly related to the osteogenic differentiation that occurs in vascular calcification are marked with an asterisk (*).

Fig. 5. Sequence alignments between miR-145a-5p, miR-145a-3p, miR-378a-5p and miR-378a-3p and mRNAs encoding BMP signaling proteins.

Fig. 6. MiR-145 and miR-378a abundances are reduced in the aorta of *Klotho* homozygous mutant mice. Relative miRNA levels in healthy controls ($Kl^{+/+}$ and $Kl^{kl/+}$) or *Klotho* homozygous ($Kl^{kl/kl}$) mice (**KK**) were assessed by RT PCR normalized against the corresponding U6 expression **(A-D)**. The bars represent the mean value +/- SEM and solid and hollow circles represent individual male and female values, respectively. * = $p < 0.05$, ** = $p < 0.01$.

Fig. 7. Vascular smooth muscle cell (VSMC)-specific lentivirus treatment increases mir-145 and mir-378a abundance in the aorta of *Klotho* mutant mice. A. Weaned *Klotho* mutant homozygous mice were treated with empty virus or virus bearing miR-145 or miR-378a pre-miRNAs. The miR-145a-5p **(B)**, miR-145a-3p **(C)** and miR-378a-5p **(D)**, miR-378a-3p **(E)** abundances were evaluated by real-time PCR and normalized against the corresponding U6 abundance. The bars represent the mean value +/- SEM. Solid and hollow circles represent individual male and female values, respectively. ** = $p < 0.01$.

Fig. 8. Restoring MiR-145 levels reduces the abundance of RNAs encoding BMP signaling factors and aortic calcification. Increased mir-145 abundance in *Klotho* mutant mice significantly decreased *Bmp2* **(A)** and *Smad5* **(C)** RNA levels and calcium levels **(E)**. *Smad1* **(B)** and *Smad9* **(D)** RNA levels did not change significantly. The bars represent the mean value +/- SEM. Solid and hollow circles represent individual male and female values, respectively. * = $p < 0.05$, ** = $p < 0.01$.

Fig. 9. Restoring MiR-378a levels reduces the abundance of RNAs encoding BMP signaling factors and aortic calcification. Increased mir-378a abundance in *Klotho* mutant mice significantly decreased *Bmp2* **(A)**, *Smad5* **(B)** RNA and calcium levels **(C)**. The bars represent the mean value +/- SEM. Solid and hollow circles represent individual male and female values, respectively. * = $p < 0.05$.

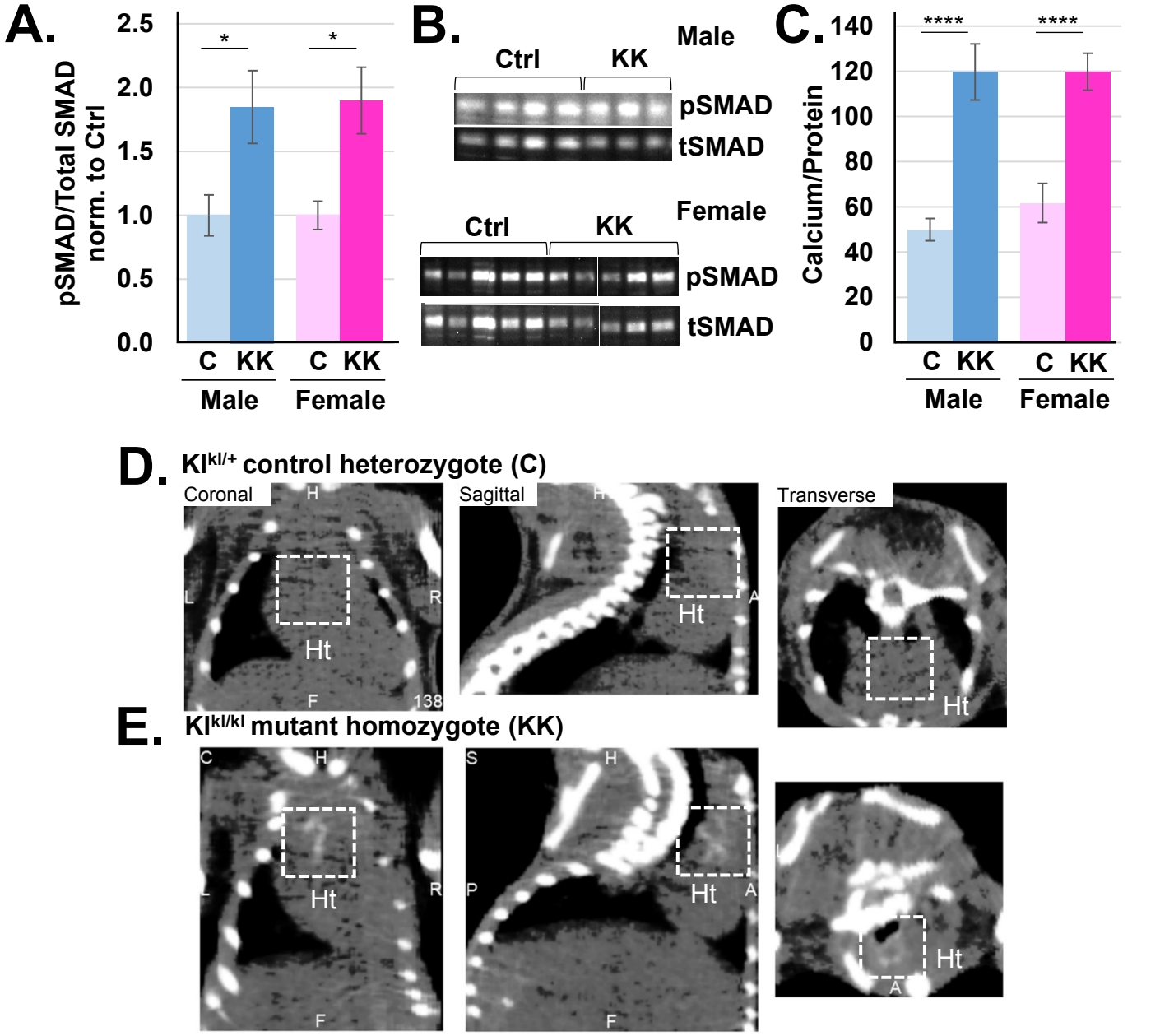

Fig. 1. BMP signaling and calcification levels in aorta from homozygous *Klotho* mutant mice. Aortas were isolated from control (C) mice with normal kidney function ($Kl^{+/+}$ and $Kl^{kl/+}$) or mice homozygous ($Kl^{kl/kl}$) for the *Klotho* mutation with renal disease (KK) between 40 and 50 days of age. Average parameter values are presented with standard error measurements (SEM). **A.** BMP signaling levels as assessed by phosphorylated SMAD1/5/9 (pSMAD) levels normalized to total SMAD1/5/9 (tSMAD) (males, n = 3 – 6; females, n = 5 – 7). **B.** Representative western blot panels showing pSMAD1/5/9 and total SMAD1/5/9 levels, males (top) and females (bottom). **C.** Average calcium levels normalized to protein concentration (males, n = 9 – 18; females, n = 6 – 7). All experiments were repeated at least twice with similar results. * $p < 0.05$, **** $p < 0.001$. **D, E.** Male littermates were scanned with an Albira PET/CT Imaging System (Carestream, Rochester, NY) set at 45 kV, 400 µA, and <35 µm voxel size. Voxel intensities in the reconstructed images were evaluated and segmented with VivoQuant image analysis software (version 1.23, inviCRO LLC, Boston MA). The dashed white lines mark mineralized areas of the aortic sinus and ascending aorta present in the heart (**Ht**) of the *Klotho* mutant homozygote **(E)**, but not in the heterozygous control $Kl^{kl/+}$ **(D)**.

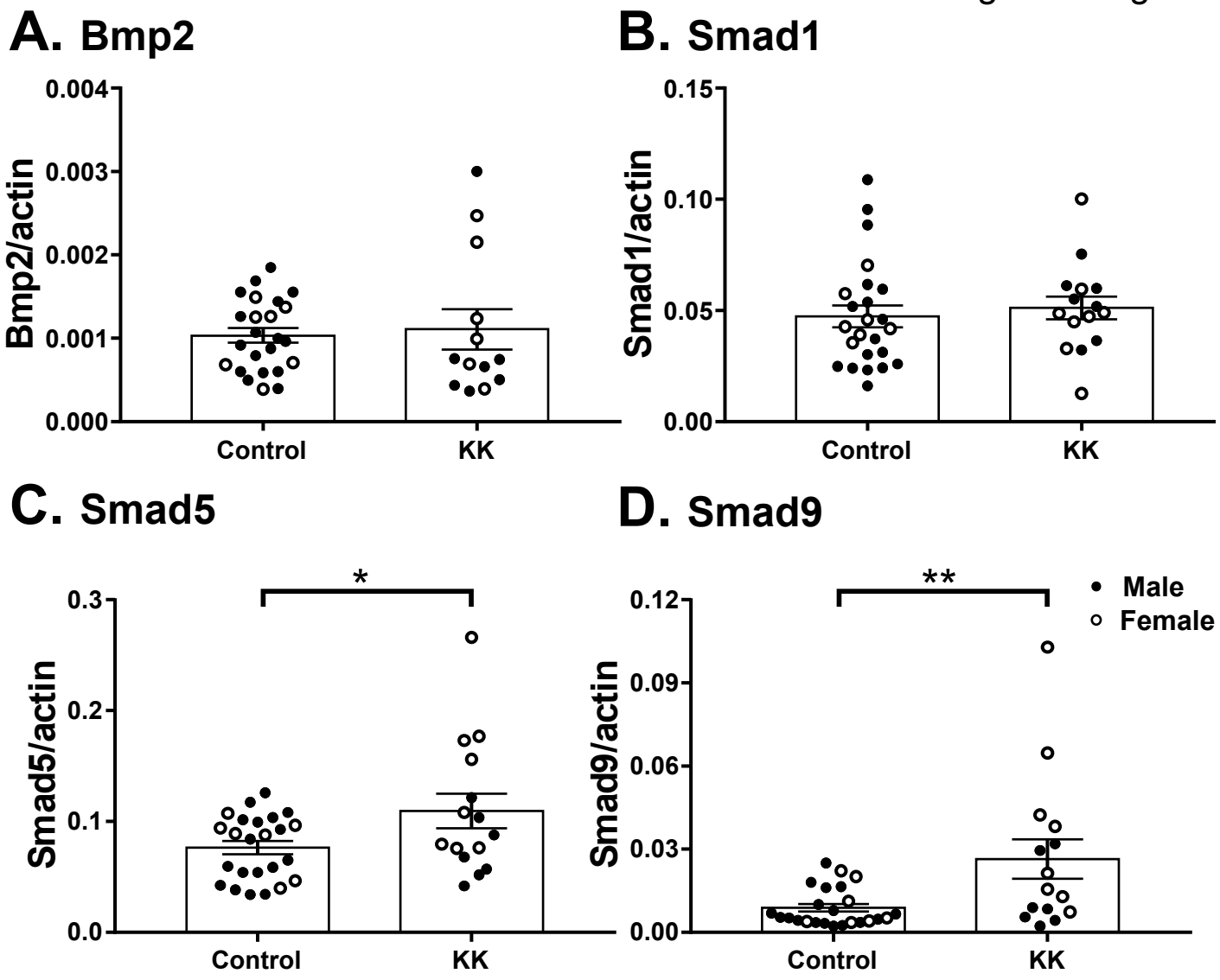

Fig. 2. *Bmp2* and *Smad1, 5,* and *9* mRNA abundances in aorta from control and homozygous *Klotho* mutant mice. Aortas were isolated from control mice bearing the wild type ($Kl^{+/+}$) or heterozygous ($Kl^{kl/+}$) *Klotho* genotypes, or diseased (KK) homozygous ($Kl^{kl/kl}$) *Klotho* mice between 40 and 50 days of age. *Klotho* mutant homozygous mice had pathologically calcified aorta. *Bmp2* **(A)** and *Smad1* **(B)** RNA levels did not change. *Smad5* **(C)** and *9* **(D)** RNA levels were significantly increased relative to control mice. The bars indicate the mean value +/- SEM. Solid and hollow circles represent individual male and female values, respectively. * = $p < 0.05$, ** = $p < 0.01$.

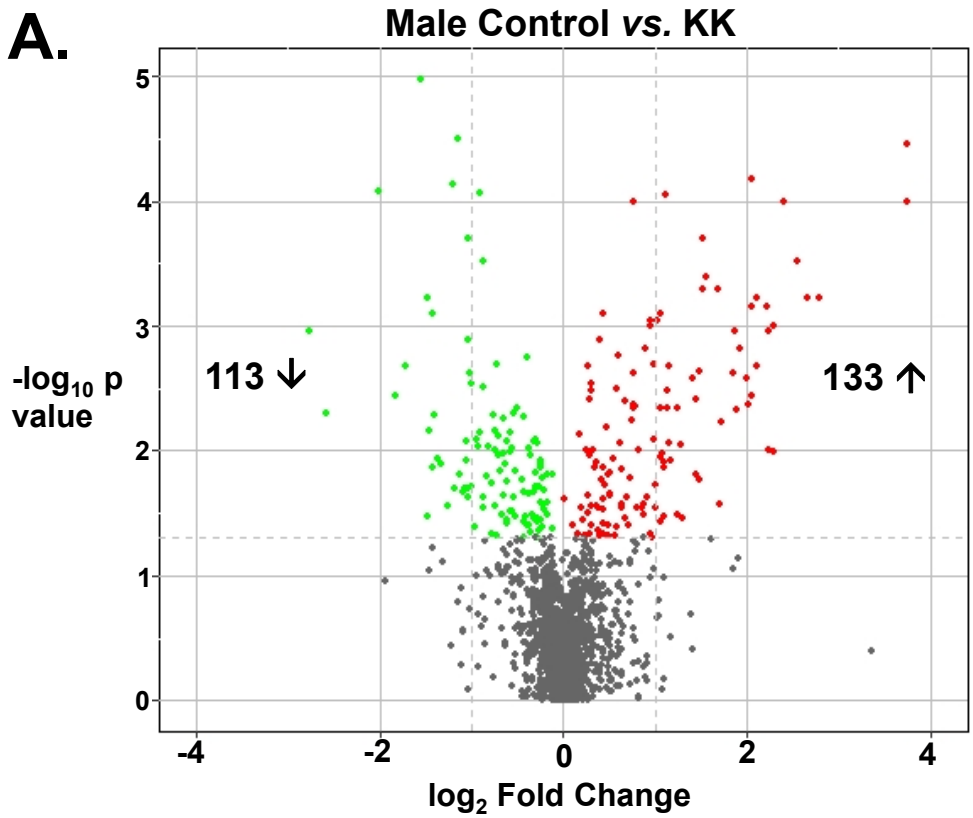

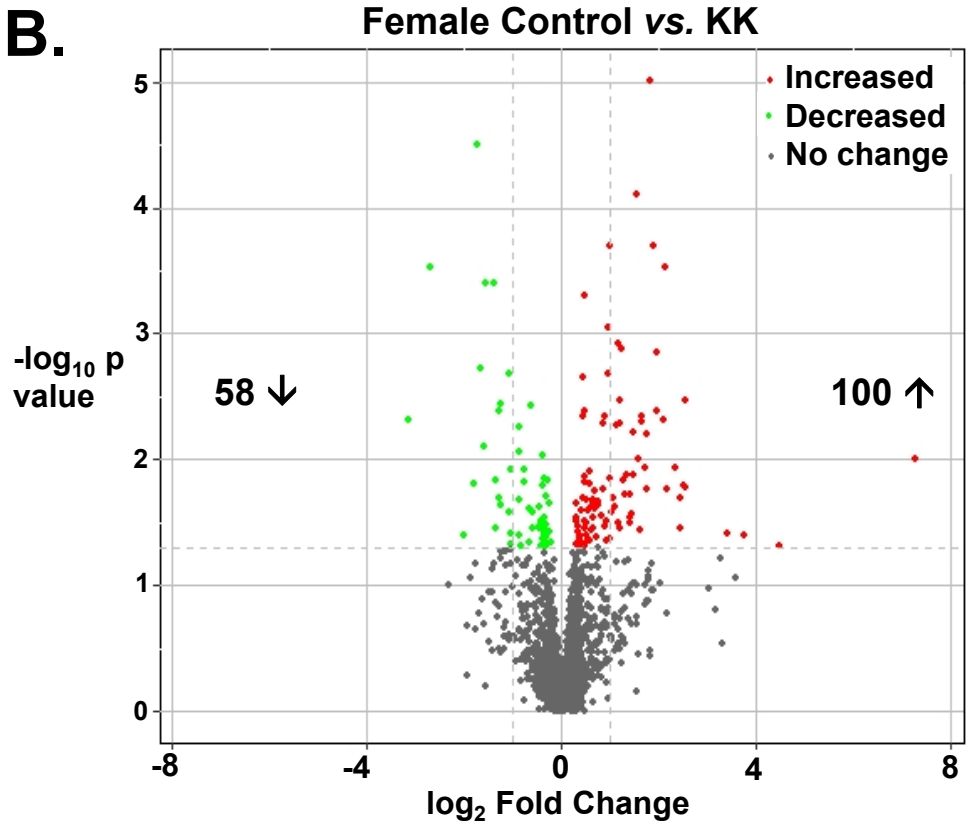

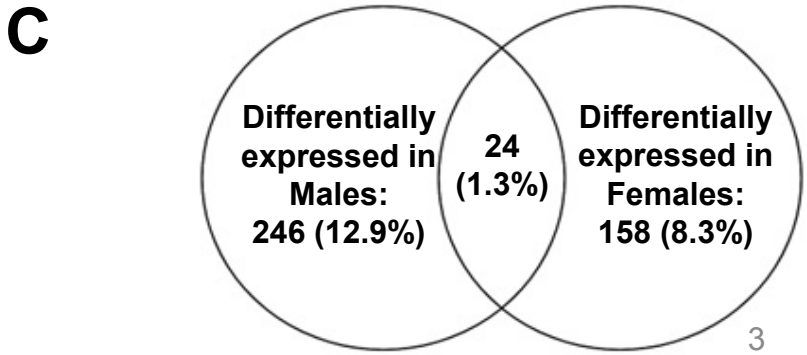

Fig. 3. MicroRNA profiles in the aorta from control and *Klotho homozygous (KK)* mutant mice. RNA was extracted from the aorta of healthy controls ($Kl^{+/+}$ and $Kl^{kl/+}$) or *Klotho* homozygous ($Kl^{kl/kl}$) mice (KK). Samples were assayed using Affymetrix miRNA version 4.0. Data analysis was performed after Robust Multi-Array Average (RMA) normalization with Transcriptome Analysis Console (TAC). **A, B.** Volcano plots illustrate miRNAs whose abundances differed significantly in aorta from diseased mice compared to control mice ($p < 0.05$). The X axis indicates $\log_2$ fold change and the Y axis indicates $-\log_{10}$ p value. Vertical dotted lines indicate 2-fold change. **C.** The Venn diagram shows the number and percentage of miRNAs differentially expressed in male or female mice or in both out of 1908 miRNAs.

Tang *et al.* Fig. 4

Legend see next page

Fig. 4. KEGG (Kyoto Encyclopedia of Genes and Genomes) and Gene Ontology (GO) analyses of miRNAs down-regulated in both sexes of *Klotho* homozygous mutant mice. The genes potentially targeted by down-regulated miRNAs were predicted by DIANA TOOLS. **A.** Target genes were grouped into gene pathways using the KEGG database. The y-axis represents the name of the KEGG pathway, and the x-axis represents the number of the genes in a certain pathway. **B.** Target genes were grouped into GO molecular function terms using the GO database. The y-axis represents the name of the GO molecular function term, and the x-axis represents the number of genes associated with each GO molecular function term. Low p adjust values are in red and high p adjust values are in blue. GO terms and KEGG pathways that are directly related to the osteogenic differentiation that occurs in vascular calcification are marked with an asterisk (*).

Predicted mmu-miR-145a target sites		Tools	Conservation of site
mu***Bmp2*** 3' UTR **miR-145a-5p**	737 5'...GGGAAUAAUUAGGAAAACUGUGAC... | || | ||||||||| || 3' UCCCUAAGGACCCUUUUGAC-CUG	Miranda	Within rodents
mu***Bmp2*** 3' UTR **miR-145a-3p**	580 5'...AUAUUCUUCAAUUCUCAGGAAU... ||| :||||||| 3' GUUCUUGUCAUAAAGGUCCUUA	Miranda	Between rodents, humans, and chicken
mu***Bmp2*** 3' UTR **miR-145a-3p**	748 5'...GGAAAACUGUGACUAUGUCAGGAAG... | :|||||| 3' GUUCUUGUCAUAAAGGUCCUUA	Miranda	Within rodents
mu***Smad1*** 3' UTR **miR-145a-5p**	1187 5'...GCAGGGUUUUUCUCUACUGGAAA... |||||| 3' UCCCUAAGGACCCUUUUGACCUG	Targetscan	Between rodents, mammals, and birds
mu***Smad5*** 3' UTR **miR-145a-5p**	234 5'...UUAGCAUUGAUCUUAAACUGGAA... ||||||| 3' UCCCUAAGGACCCUUUUGACCUG	Targetscan	Between mammals
mu***Smad9*** 3' UTR **miR-145a-5p**	754 5'...GAGAUGAAGCUGUAG-ACUGGAAG... ||| ||||||| 3' UCCCUAAGGACCCUUUUGACCUG	Targetscan	Within rodents
Predicted mmu-miR-378 target sites			
mu***Bmp2*** 3' UTR **miR-378a-5p**	579 5'...UAUAUUCUUCAAUUCUCAGGAAU... |||||| 3' UGUGUCCUGGACCUCAGUCCUC	Miranda Targetscan	Between rodents, mammals, and birds
mu***Bmp2*** 3' UTR **miR-378a-5p**	751 5'...AAACUGUGACUAUGUCAGGAA... ||||||| 3' UGUGUCCUGGACCUCAGUCCUC	Miranda Targetscan	Within rodents
mu***Bmp2*** 3' UTR **miR-378a-3p**	508 5'...GUUCACAAGUUCAAGUCCAAA... | |:|||||||| 3' GGAAGACUGAGGUUCAGGUCA	Miranda	Between rodents and humans
mu***Smad5*** 3' UTR **miR-378a-5p**	1156 5'...UUUACUUGGCAGCCUUCAGGAAC... |||||| 3' UGUGUCCUGGACCUCAGUCCUC	Targetscan	Within rodents

Fig. 5. Sequence alignments between miR-145a-5p, miR-145a-3p, miR-378a-5p and miR-378a-3p and mRNAs encoding BMP signaling proteins.

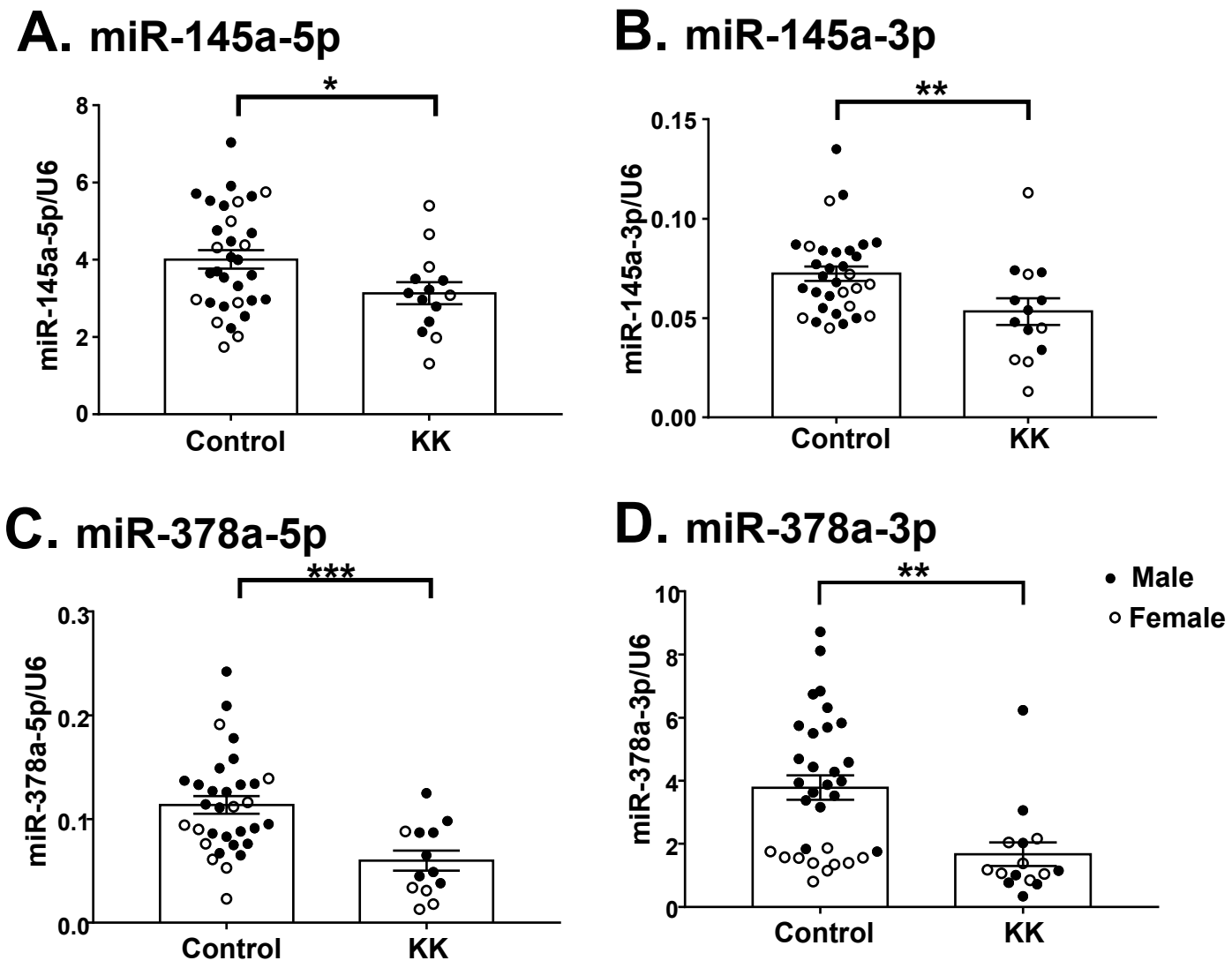

Fig. 6. MiR-145 and miR-378a abundances are reduced in the aorta of *Klotho* homozygous mutant mice. Relative miRNA levels in healthy controls ($Kl^{+/+}$ and $Kl^{kl/+}$) or *Klotho* homozygous ($Kl^{kl/kl}$) mice (**KK**) were assessed by RT PCR normalized against the corresponding U6 expression **(A-D)**. The bars represent the mean value +/- SEM and solid and hollow circles represent individual male and female values, respectively. * = $p < 0.05$, ** = $p < 0.01$.

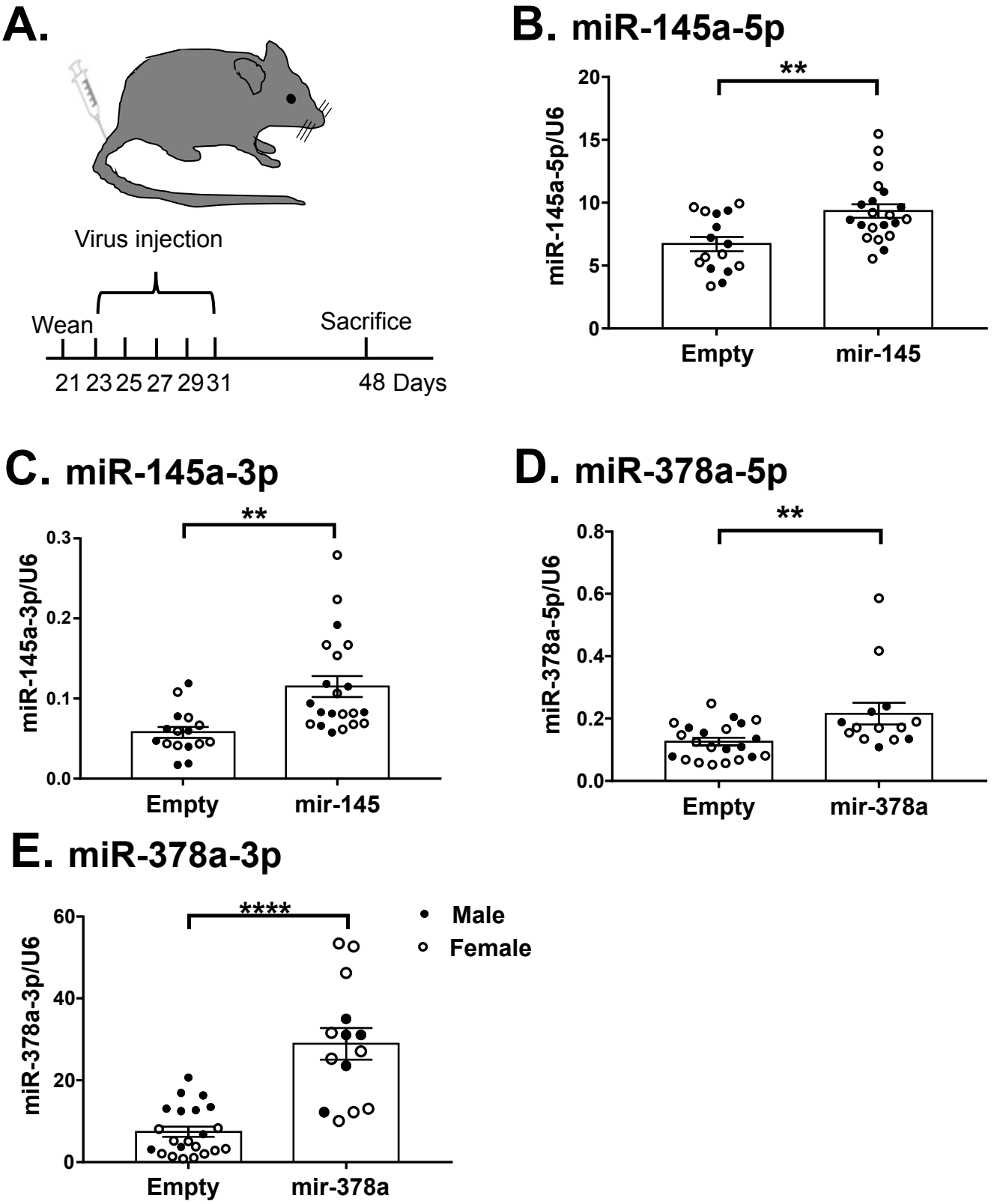

Fig. 7. Vascular smooth muscle cell (VSMC)-specific lentivirus treatment increases mir-145 and mir-378a abundance in the aorta of *Klotho* mutant mice. A. Weaned *Klotho* mutant homozygous mice were treated with empty virus or virus bearing miR-145 or miR-378a pre-miRNAs. The miR-145a-5p **(B)**, miR-145a-3p **(C)** and miR-378a-5p **(D)**, miR-378a-3p **(E)** abundances were evaluated by real-time PCR and normalized against the corresponding U6 abundance. The bars represent the mean value +/- SEM. Solid and hollow circles represent individual male and female values, respectively. ** = $p < 0.01$.

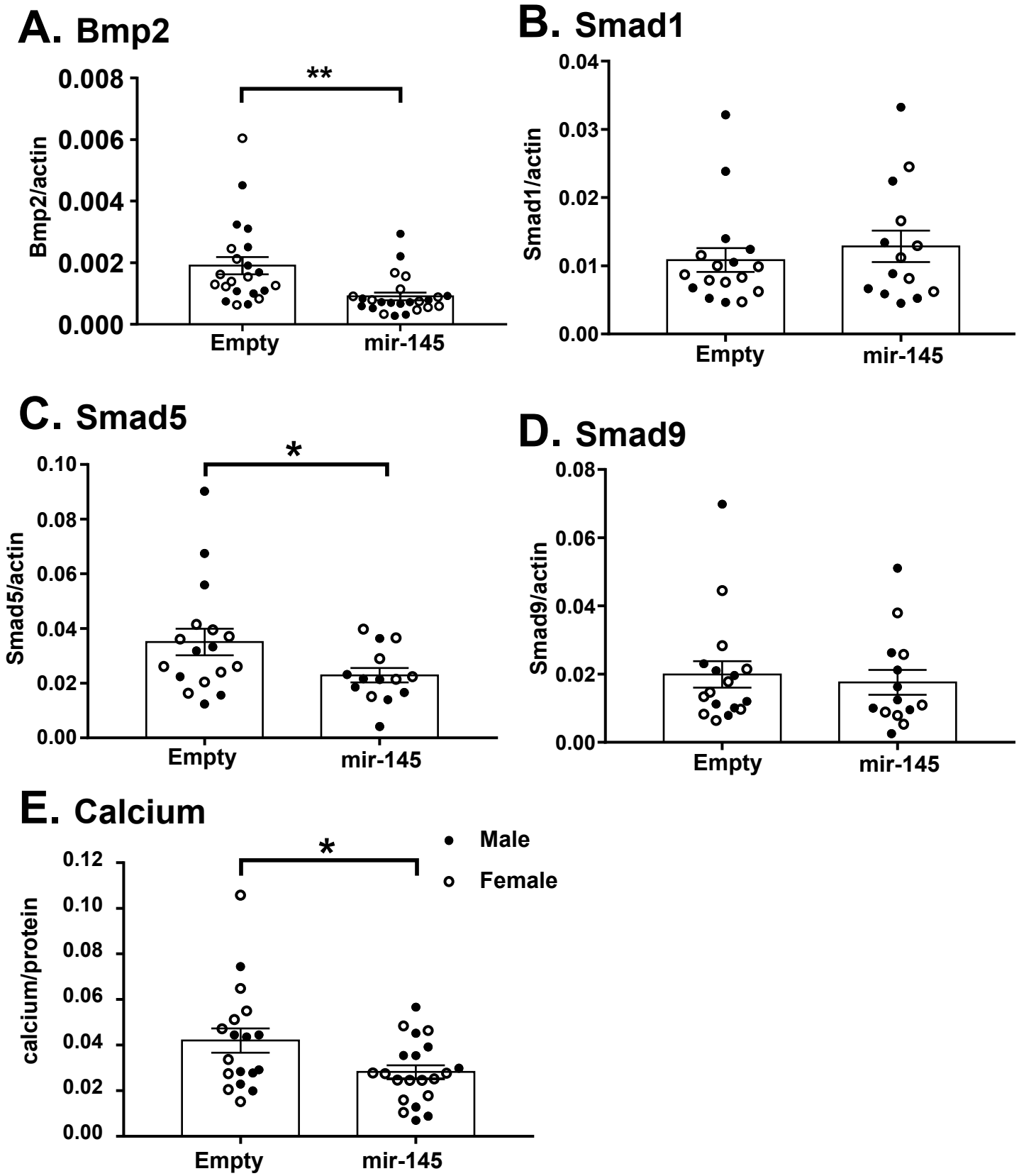

Fig. 8. Restoring MiR-145 levels reduces the abundance of RNAs encoding BMP signaling factors and aortic calcification. Increased mir-145 abundance in *Klotho* mutant mice significantly decreased *Bmp2* **(A)** and *Smad5* **(C)** RNA levels and calcium levels **(E)**. *Smad1* **(B)** and *Smad9* **(D)** RNA levels did not change significantly. The bars represent the mean value +/- SEM. Solid and hollow circles represent individual male and female values, respectively. * = $p < 0.05$, ** = $p < 0.01$.

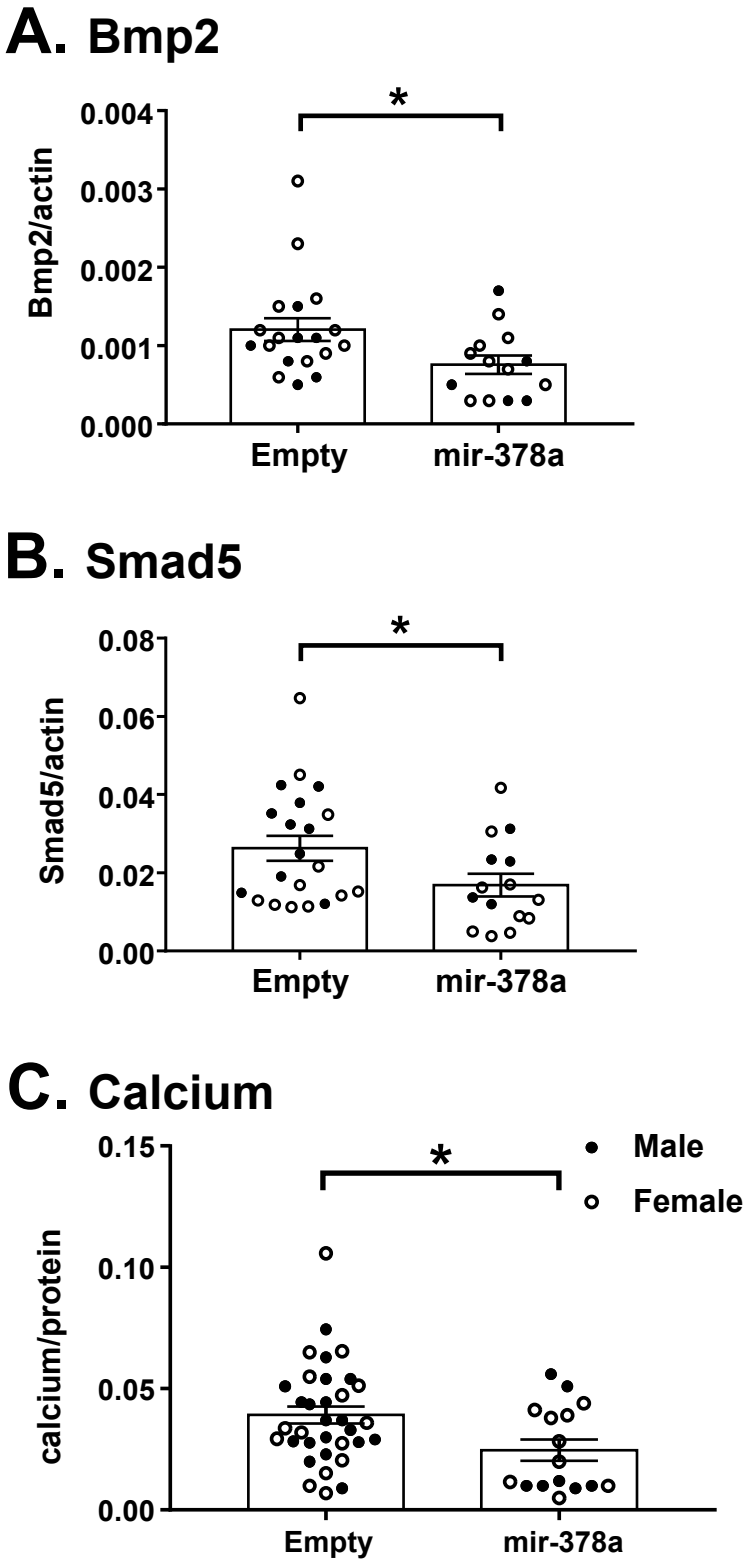

Fig. 9. Restoring MiR-378a levels reduces the abundance of RNAs encoding BMP signaling factors and aortic calcification. Increased mir-378a abundance in *Klotho* mutant mice significantly decreased *Bmp2* **(A)**, *Smad5* **(B)** RNA and calcium levels **(C)**. The bars represent the mean value +/- SEM. Solid and hollow circles represent individual male and female values, respectively. * = $p < 0.05$.